HHS Public Access

Author manuscript

Mol Cancer Ther. Author manuscript; available in PMC 2020 August 01.

Published in final edited form as:

Mol Cancer Ther. 2020 February ; 19(2): 397–408. doi:10.1158/1535-7163.MCT-19-0319.

The novel glutamine antagonist prodrug JHU395 has antitumor activity in malignant peripheral nerve sheath tumor

Kathryn M. Lemberg[1,2], **Liang Zhao**[1], **Ying Wu**[2], **Vijayabhaskar Veeravalli**[2,3], **Jesse Alt**[2], **Joanna Marie H. Aguilar**[2], **Ranjeet P. Dash**[2,3], **Jenny Lam**[2], **Lukáš Tenora**[6], **Chabely Rodriguez**[2], **Michael T. Nedelcovych**[2,3], **Cory Brayton**[4], **Pavel Majer**[6], **Jaishri O. Blakeley**[1,3], **Rana Rais**[2,3], **Barbara S. Slusher**[1,2,3,5,*]

[1]Department of Oncology, Johns Hopkins School of Medicine; Baltimore MD 21205; USA.

[2]Johns Hopkins Drug Discovery, Johns Hopkins School of Medicine; Baltimore MD 21205; USA.

[3]Department of Neurology, Johns Hopkins School of Medicine; Baltimore MD 21205; USA.

[4]Department of Molecular and Comparative Pathobiology, Johns Hopkins School of Medicine; Baltimore MD 21205; USA.

[5]Departments of Psychiatry, Neuroscience, and Medicine; Johns Hopkins School of Medicine; Baltimore MD 21205; USA.

[6]Institute of Organic Chemistry and Biochemistry, Czech Academy of Sciences, Flemingovo n. 2, Prague 166 10, Czech Republic.

Abstract

The carbon and nitrogen components of glutamine are used for multiple biosynthetic processes by tumors. Glutamine metabolism and the therapeutic potential of glutamine antagonists (GA), however, are incompletely understood in malignant peripheral nerve sheath tumor (MPNST), an aggressive soft tissue sarcoma observed in patients with neurofibromatosis type I. We investigated glutamine dependence of MPNST using JHU395, a novel orally-bioavailable GA prodrug designed to circulate inert in plasma, but permeate and release active GA within target tissues. Human MPNST cells, compared to Schwann cells derived from healthy peripheral nerve, were selectively susceptible to both glutamine deprivation and GA dose-dependent growth inhibition. *In vivo*, orally administered JHU395 delivered active GA to tumors with over two-fold higher tumor-to-plasma exposure, and significantly inhibited tumor growth in a murine flank MPNST model without observed toxicity. Global metabolomics studies and stable isotope labeled flux analyses in tumors identified multiple glutamine dependent metabolites affected, including prominent effects

[*]**Corresponding Author Contact Information:** Barbara Slusher, Ph.D.; Johns Hopkins School of Medicine; Rangos Suite 277; 855 North Wolfe Street; Baltimore MD 21205. Phone: 410-614-0662. Fax: 410-614-0659. bslusher@jhmi.edu.

Conflict of Interest/Disclosure Statement: JHU395 is licensed to Dracen Pharmaceuticals, a company pursuing small molecule glutamine antagonists for oncology and immunometabolic applications. Under a license agreement between Dracen Pharmaceuticals, Inc. and the Johns Hopkins University, Dr. Slusher, Dr. Rais, and Mr. Alt are entitled to royalty distributions related to technology used in the research described in this publication. Similarly under a license agreement between Dracen Pharmaceuticals, Inc. and the IOCB, Dr. Majer and Dr. Tenora are entitled to royalty distributions related to technology used in the research described in this publication. Drs. Slusher, Rais, and Majer are also co-founders of and hold equity in Dracen Pharmaceuticals, Inc. Dr. Nedelcovych served as a consultant to Dracen Pharmaceuticals. These arrangements have been reviewed and approved by the Johns Hopkins University and the IOCB in accordance with institutional conflict of interest policies. The remaining co-authors declare no conflicts of interest.

on purine synthesis. These data demonstrate that glutamine antagonism is a potential antitumor strategy for MPNST.

Keywords

glutamine; prodrug; 6-diazo-5-oxo-L-norleucine; malignant peripheral nerve sheath tumor; NF1

[1]Introduction

Tumor cells use glutamine to build molecules needed for proliferation and survival (1, 2) including: direct protein synthesis; abstraction of the gamma amido group by glutamine amidotransferases for nucleotide, hexosamine, amino acid, and coenzyme synthesis; and incorporation of the carbon skeleton to the tricarboxylic acid (TCA) cycle following glutaminolysis (3). Alterations in tumor glutamine metabolism have been observed across multiple tumor types and linked to multiple oncogenes and tumor suppressors including *MYC* (4), *KRAS* (5), *TP53* (6), and *PTEN* (7). Glutamine utilization is also dependent on tumor cell environment and differs between cell culture and *in vivo* models (8, 9).

MPNST is a rare aggressive soft tissue sarcoma originating from Schwann cells. MPNST can occur sporadically, as a secondary malignancy, or in up to 15% of people with the syndrome neurofibromatosis type I (NF1) (10, 11). NF1 is an autosomal dominant condition caused by germline loss of one copy of the RAS-GAP *NF1* and presents with a wide range of manifestations including multiple cancers (12). MPNST is poorly responsive to chemotherapy and radiation therapy, and the only chance for long term survival is if the lesion is completely resected with wide margins (13, 14). As MPNST most often develops in critical, deep areas such as major nerve plexi, this is rarely feasible and hence there is an outsized chance of mortality from MPNST versus other sarcomas (15).

Small molecule glutamine antagonists (GA) are valuable tools for studying glutamine metabolism and have garnered interest as antitumor therapeutics. 6-diazo-5-oxo-L-norleucine (DON) and its naturally occurring prodrug azotomycin are diazo analogs of glutamine that irreversibly inhibit multiple glutamine-utilizing enzymes. GA have been observed to cause decreased proliferation or induction of apoptosis, depending on genetic context, cell/tissue type, and environment (16, 17, 18). GA have been tested clinically (19), including for sarcomas (20). Unfortunately, their clinical development was hampered by use of high intermittent dosing regimens poorly suited to a metabolic inhibitor (19, 21) and gastrointestinal (GI) toxicity, as the GI system is highly glutamine utilizing (22). We recently developed targeted GA prodrugs around the parent compound DON in attempt to decrease DON exposure to sites of toxicity (e.g. gut) and preferentially deliver DON to target tissues (e.g. nervous tissues, tumors) (23–25). One such targeted GA termed JHU395 (previously 13d) contains (phenyl(pivaloyloxy)methoxy)carbonyl and isopropyl ester modifications to the amine and carboxylate groups of DON, respectively, which significantly increase its lipophilicity relative to DON (clogP 2.75 vs −2.5) (Figure 1C) (23). Prior

[1]**Abbreviations:** glutamine antagonist (GA), 6-diazo-5-oxo-L-norleucine (DON), malignant peripheral nerve sheath tumor (MPNST), neurofibromatosis type 1 (NF1), C57BL6/NHsd mice (B6), formylglycinamide ribonucleotide (FGAR)

investigation of JHU395 demonstrated that the prodrug remains intact in swine and human plasma (83–88% at 1 hour) (23). When directly compared to an equimolar dose of DON administered to swine, JHU395 resulted in significantly lower DON exposure in plasma ($AUC_{0\rightarrow t}$ 29.9 nmol•hr/ml vs 5.7 nmol•hr/ml), leading to a nearly 10-fold enhancement of the DON brain-to-plasma ratio (DON brain-to-plasma 0.148; JHU395-derived DON brain-to-plasma 1.38; ratio 9.3) (23). Our group has also identified other GA prodrugs with enhanced DON CSF-to-plasma ratio in non-human primates (compound 5c, DON CSF-to-plasma ratio 0.038; 5c-derived DON CSF-to-plasma ratio 0.28; ratio 7.6) (24) as well as GA prodrugs with enhanced DON exposure to lymphoid tumors versus GI tissues in mice (prodrug 6, tumor $AUC_{0\rightarrow t}$=5.1 nmol•h/g; GI $AUC_{0\rightarrow t}$=0.45 nmol•h/g; ratio 11) (25). Thus prodrug GA may enable improved delivery of active DON to target tissues while avoiding sites of toxicity, enabling better tolerability and translation of this metabolic therapy.

There has been interest in metabolic inhibitors as therapies for MPNST (26), but glutamine metabolism has only been explored using the selective glutaminase inhibitor CB-839 (27). We hypothesized that a broadly active GA with target tissue penetration could provide further insight into MPNST glutamine metabolism. Compared to immortalized healthy Schwann cells, we found that human NF1-associated MPNST cells were sensitive to glutamine deprivation and antagonism. JHU395 was stable in human plasma and delivered DON to human MPNST cells in culture and to a murine flank MPNST. We then identified a daily oral dosing regimen of JHU395 that was well tolerated and delivered micromolar levels of DON to tumor in the murine MPNST model. Chronic JHU395 administration significantly decreased MPNST growth without overt GI- or neuro-toxicities. In vivo metabolomics analyses on JHU395-treated tumors identified multiple glutamine dependent metabolites affected, including prominent effects on purine synthesis. Our results support further evaluation of GA as a novel therapeutic approach to prevent MPNST growth.

Materials and Methods

Cell culture

MPNST cell lines (sNF96.2, sNF02.2) were obtained from American Type Culture Collection. ipn02.32λ (28) was shared from NCATS (M. Ferrer) and validated by STR Cell Line Authentication (Johns Hopkins GRCF). For establishment of flank MPNST, cells harvested from a tumor in an NPcis (*NF1*$^{+/-}$;*p53*$^{+/-}$) mouse (29) and frozen in 5% DMSO, were a kind gift from Dr. Verena Staedtke (Johns Hopkins). Cells were cultured in DMEM (ThermoFisher 119965), 10% fetal bovine serum (Hyclone SH30073.1), and 1% penicillin/streptomycin (ThermoFisher). Cells were incubated at 37°C, in a humidified atmosphere with 5% CO_2. Confluency was monitored using an Axiovert 25 optical microscope.

Cell growth in low glutamine was studied by plating 25,000 sNF96.2 cells/well in standard media in 6-well culture dishes. The next day media was replaced with low glutamine media (ThermoFisher DMEM #10313–021). Each subsequent day cells were removed from the plate using 0.05% trypsin and live cell concentration was determined by trypan blue exclusion using a BioRad TC20 hemacytometer. Dose response titration of glutamine was measured in a 96 well plate by alamar blue fluorescence at 590 nm (ThermoFisher DAL1025). 1500–2000 cells per well were plated in standard media. One day later media

was exchanged for glutamine-free media (prepared with dialyzed FBS, ThermoFisher A3382001); fixed concentrations of glutamine were added across the plate and cells were incubated for 72 hours prior to dye addition. Dose response curves for DON and JHU395 (synthesized according to ref. 23) were generated similarly in standard media or media containing added purine nucleotides (guanosine monophosphate, 100μM). Curve fitting and EC_{50}/IC_{50} values were determined in GraphPad Prism. Data shown is representative of at least two independent experiments.

Oxygen consumption

Oxygen consumption rate was measured using a Seahorse XFe96 Analyzer (Agilent). sNF96.2 cells were seeded at 20,000 cells/well in 96 well XF flux plates 48 hours prior to the study. The next day media was exchanged for media containing vehicle, DON or JHU395 (10 μM), or glutamine-free condition. On the day of the assay, oxygen consumption rate was measured during the XF Mito Stress Test (Agilent) according to the manufacturer's directions. At least 6 wells were measured per condition; recordings of less than zero in a given well were imputed as zero for data analysis. Data shown is representative of two independent experiments. Calculated rates of respiration were performed based on the equations given in (30).

Mouse models and JHU395 treatment

Experimental procedures were approved by the Johns Hopkins University Animal Care and Use Committee and were consistent with the Guide for the Care and Use of Laboratory Animals (31). C57BL6/NHsd (B6) or CD-1 male mice, at 12 weeks of age between 25 and 30 g were obtained from Envigo. NPcis (B6;129S2-*Trp53*^{tm1Tyj} *Nf1*^{tm1Tyj}/J) transgenic mice (29) were a kind gift from Dr. Verena Staedtke (Johns Hopkins) and were genotyped using previously validated primers on ear punches (Transnetyx).

For dose tolerance in NPcis mice, male and female non-tumored double heterozygote (*NF1*$^{+/-}$;*p53*$^{+/-}$) 12 week old mice were treated daily with vehicle (phosphate buffered saline (PBS) + 1% Tween-80 and 2.5% ethanol p.o., n=3) or JHU395 (1.2 mg/kg p.o. × 5 days, 0.5 mg/kg p.o. × 27 days, n=5). Animals were weighed 3 times per week, and percent change from baseline weight was calculated.

To form tumors in B6, 3–6 × 10^6 murine NPcis tumor cells harvested from cell culture were washed twice in PBS, resuspended in 0.2 ml PBS, and injected subcutaneously to the right flank. Tumors developed over 21–28 days. A subset of untreated tumors (n=4) were processed for histologic characterization and evaluated (see below).

For efficacy studies, mice with average tumor volume 300 mm^3 as measured by calipers were used; tumor volume was calculated by the formula: Volume = $(L \times (W^2))/2$. Animals were treated daily for fourteen days with vehicle (PBS + 1% Tween-80 + 2.5% ethanol) or JHU395 (1.2 mg/kg × 5 days, 0.5 mg/kg × 9 days) administered by oral gavage. Animal weights and tumors were measured thrice weekly and on the final experimental day. The study shown was stopped after fourteen days as one animal in the vehicle cohort had tumor growth beyond institutional standards and one animal in the JHU395 cohort was found deceased after losing approximately 10% body weight. Animals were euthanized by CO_2

inhalation followed by cardiac puncture to collect blood for clinical pathology. Additional tissues of interest (tumor, brain, jejunum) were harvested and either flash frozen in liquid nitrogen or preserved for histology. Efficacy data is representative of three independent experiments.

Histology and immunohistochemistry

Harvested tissues from naïve, vehicle, or JHU395 treated mice (n = 3–4/condition) were fixed overnight in 10% neutral buffered formalin, then transferred to 70% ethanol. Fixed tissues were routinely processed to paraffin. Sections (~5 μm) were stained with hematoxylin and eosin (H&E), and examined by a veterinary pathologist (author C.B.). Image capture was performed on a Nikon 55i photomicroscope, with 1.2× C-mount adapter, (Nikon Inc) Spot Flex camera, and Spot imaging software v5.1 (Diagnostic Instruments, Inc), and from slides scanned on an Aperio ScanScope CS scanner (Leica Biosystems).

Ki67 and cleaved caspase-3 immunohistochemistry were performed on 5 μm thickness formalin-fixed paraffin-embedded sections on a Leica Bond RX automated stainer using Bond reagents (Leica Biosystems) and following standard manufacturer's instructions except for the following details. For Ki67, heat-induced epitope retrieval was performed in a pH 9.0 buffer, and anti-Ki67 rabbit monoclonal antibody (clone SP6, ab16667, Abcam) was applied at a concentration of 1:100. For cleaved caspase-3, heat induced epitope retrieval was performed in a pH 6.0 buffer, and anti-cleaved caspase 3 rabbit polyclonal antibody (Cell Signaling Tecnology #9661) was applied at a concentration of 1:250. These were followed by application of a polymer detection system (DS9800, Novocastra Bond Polymer Refine Detection, Leica Biosystems). The chromogen was 3,3 diaminobenzidine tetrachloride; sections were counterstained with hematoxylin. Analysis of scanned slides was performed using ImageScope (Lecia Biosystems).

Western blotting

Cells were cultured as above, treated as indicated on figures, and harvested with 0.05% trypsin. Cells were washed with cold PBS, then lysed using RIPA buffer (Pierce) with protease/phosphatase inhibitors. 20–30 μg of protein per well was separated by 4–12% Bis-Tris SDS/PAGE (ThermoFisher) and transferred by iBlot (Invitrogen) to PVDF membrane. Rabbit anti-phospho-ERK1/2 (#4370S), total ERK (#4695S), cleaved PARP (#9541), and mouse anti-beta-tubulin (#86298T) were purchased from Cell Signaling Technologies. Detection was accomplished with Licor IRDye 800cw goat anti-rabbit (925–32211) and IRDye 680RD goat anti-mouse (925–68070) secondary antibodies using an Odyssey Scanner.

Parallel Artificial Membrane Permeation Assay (PAMPA)

PAMPA (32) was conducted by Cyprotex LLC (MA, USA) and samples were shipped to JHU for analysis. Pre-coated PAMPA plates were purchased from BD Biosciences (Product #353015). DON or JHU395 stock solution was prepared by diluting a 20 mM DMSO stock in phosphate buffered saline (PBS), pH 7.0 to give a final concentration of 20 μM. DON, JHU395 or verapamil (high permeability positive control) solutions (300 μL) were added to the donor plate. PBS buffer pH 7.0 (200 μL) was added to each well of the acceptor plates.

The acceptor filer plate was carefully placed onto the donor plate to create a sandwich. Plates were incubated undisturbed at room temperature for 5 h. Donor and acceptor samples for prodrugs and positive control were quantified by LC-MS/MS as described below (23–25).

The apparent permeability (P_{app}) is calculated using the equation (1):

$$P_{app} = ((V_D \times V_A)/((V_D + V_A) \times A \times t)) \times -\ln\left(1 - \left(\left[drug_{acceptor}\right]/\left[drug_{equilibrium}\right]\right)\right) \quad (1)$$

where P_{app} is the permeability; V_D and V_A are the volumes of the donor and acceptor compartments, A is the area of the membrane, and t is the incubation time in seconds (32).

Tumor cell partitioning

Tumor cell-to-plasma partitioning was conducted using sNF96.2 or P493B human cancer cells harvested from cell culture and centrifuged (1000 rpm, 5 min, 25°C). The pellet was washed twice in PBS followed by centrifugation and resuspended in human plasma (Innovative Research, USA) to obtain a cell density of 7.5 million cells/mL. 1 mL of cell-plasma suspension was spiked with JHU395 (20μM) and incubated at 37°C for 1 hour. Following centrifugation (1000 × g, 5 min, 4°C), plasma was collected and stored at −80°C. The cell pellet was washed once with ice cold PBS, centrifuged, and stored at −80°C until liquid chromatography-mass spectrometry (LC-MS/MS) analysis as described previously (23–25).

JHU395 Pharmacokinetic Analysis

B6 flank MPNST, non-tumored B6 control, or CD-1 mice received 1.2 mg/kg p.o. JHU395 prepared in PBS + 1% Tween-80 + 2.5% ethanol. At indicated times post drug administration mice were euthanized (n=3–5 mice/time point). Blood samples were collected in heparinized microtubes by cardiac puncture and centrifuged (3000 × *g*, 10 min.) Plasma (~300 μL) was collected in polypropylene tubes. Xenograft tumors and GI tissues were dissected, and all tissues were stored at −80°C until bioanalysis. DON was extracted from plasma or tissue samples by protein precipitation. 5 μL of methanol containing 10 μM glutamate-d5 (internal standard) was added per μL of plasma or mg of tissue. Tissue samples were homogenized and centrifuged (16,000 × g, 5 min.) Supernatants were derivatized using dabsyl chloride and analyzed by LC-MS/MS as previously described (23–25).

Quantitative glutamine analysis

Tumor and plasma glutamine were quantified similarly to our previous description (24). B6 flank MPNST mice or non-tumored B6 controls were administered vehicle or oral JHU395 (1.2 mg/kg) once thirty minutes before euthanasia. Tumors were snap frozen in liquid nitrogen; whole blood was centrifuged and plasma frozen on dry ice. Metabolite extraction was performed as described for DON bioanalysis. Standard concentration curves of glutamine in untreated tumor tissue and mouse plasma were prepared (0.01–10 μmol/ml or μmol/g). For quantification, supernatants (4 μL) were injected and separated on an Agilent 1290 HPLC equipped with a Waters Acquity UPLC BEH Amide 1.7 μm 2.1 × 100 mm

HILIC column at a flow rate of 0.3 mL/minute coupled to an Agilent 6520 mass spectrometer. Glutamine content was averaged by group and analyzed by t-test.

Modified Irwin assay

B6 flank MPNST mice were treated with vehicle or JHU395 (n=11/group) using the dosing regimen described for efficacy experiments. Autonomic and somatomotor behaviors were scored based on the modified Irwin assay (33) on days 0, 8, and 15 of the dosing period. The observer was blinded to treatment groups. As an assay control, a cohort of n = 5 non-tumored mice received the muscarinic acetylcholine receptor agonist oxotremorine (0.5 mg/kg s.c.) once thirty minutes prior to behavioral testing. Scores were averaged and normalized to controls at the start of the assay.

Metabolomics Analysis

B6 flank MPNST mice (n = 8/group) were treated with vehicle or JHU395 (1.2 mg/kg/dose p.o.) for five days. On the day of tumor harvest, mice were administered drug orally and euthanized two hours later. Tumors were harvested and flash frozen in liquid nitrogen. Global metabolite profiling on tumors was performed by Metabolon (Durham, NC) using ultra high performance liquid chromatography coupled to tandem mass spectrometry (UPLC-MS/MS). Individual samples were subjected to methanol extraction then split into aliquots for analysis. The global biochemical profiling analysis is comprised of four arms consisting of reverse phase chromatography positive ionization methods optimized for hydrophilic compounds (LC-MS Pos Polar) and hydrophobic compounds (LC-MS Pos Lipid), reverse phase chromatography with negative ionization conditions (LC-MS Neg), as well as a HILIC chromatography method coupled to negative ionization (LC-MS Polar) (34). All of the methods alternated between full scan MS and data dependent MS^n scans. The scan range varied slightly between methods but generally covered 70–1000 m/z. Metabolites were identified by automated comparison of the ion features in the experimental samples to a reference library of chemical standard entries (35). LC-MS data on polar compounds was analyzed at Johns Hopkins using Metaboanalyst 4.0 (36) for statistical analysis. Peak intensities were log transformed and missing or zero values were imputed with half of the minimum observed value for each compound.

Quantitative formylglycinamide ribonucleotide (FGAR) analysis

Tumors harvested from B6 flank MPNST treated with either vehicle or JHU395 (1.2 mg/kg p.o.) as above were snap frozen in liquid nitrogen. Metabolites were extracted from tumor by protein precipitation. 5 μL of methanol containing 10 μM deuterated N-Acetylaspartic acid (internal standard) was added per mg of tissue. Tissue samples were homogenized and centrifuged (16,000 × g, 5 min). A standard concentration curve of FGAR (37) in untreated tumor tissue was prepared (0.3 – 1000 μmol/g). For quantification, supernatants (2 μL) were injected and separated on an UltiMate 3000 UHPLC coupled to Q Exactive Focus orbitrap mass spectrometer (Thermo Fisher Scientific Inc., Waltham MA). Samples were separated on an Agilent EclipsePlus C18 RRHD (1.8 μm) 2.1 × 100 mm column. The mobile phase consisted of 8 mM dimethylhexylamine (DMHA) + 0.005% formic acid in water, pH 9 (A), and of 8 mM DMHA in acetonitrile (B). Separation was achieved at a flow rate of 0.4 mL/min using a gradient run. Quantification was performed in Full MS negative mode. Data

were acquired and quantified with Xcalibur software. FGAR content was averaged by group and analyzed by t-test.

In vivo stable isotope flux analysis

B6 flank MPNST mice were treated with vehicle or JHU395 (1.2 mg/kg/dose p.o.) for five days. On the day of tumor harvest, mice were administered drug orally and thirty minutes later received three 0.2 ml tail vein injections of $^{15}N_2$-glutamine or $^{13}C_5$-glutamine (200 mM) every fifteen minutes. Following euthanasia, tumor tissue was harvested and flash frozen in liquid nitrogen using a biosqueezer. Metabolites were extracted in cold 80% methanol and dried by nitrogen evaporation at room temperature. Metabolites were solubilized in 50% acetonitrile:water and analyzed by LC-MS using an Agilent 1290 Infinity Binary UHPLC pump with wellplate autosampler at 4°C and a 6250 accurate-mass Q-TOF MS. Chromatography was performed following injection of 4 μl over a Zorbax Extend C18 column at 40°C by gradient elution run from 3% methanol with 5 mM tributylamine to 100% methanol with 5 mM tributylamine over 22 minutes. The MS was equipped with a dual electrospray ion source operated in negative-ion mode. Data were acquired with Agilent MassHunter Acquisition software and processed using MassHunter Profinder software. The metabolite database used for identification was developed using MassHunter PCDL Manager with retention times based on the ion-pairing method. Isotopologue peak extractions, isotope incorporation analysis, and natural abundance corrections were achieved by MassHunter Profinder.

Results

MPNST cells are sensitive to glutamine deprivation and small molecule GA.

Growth of human MPNST cells (sNF96.2) was attenuated in low glutamine media (Figure 1A). When glutamine was titrated back, MPNST cells required higher glutamine concentration (EC_{50} = 209 μM) to rescue growth compared to an immortalized Schwann cell line derived from healthy peripheral nerve (ipn02.32λ; EC_{50} = 64.5 μM) (Figure 1B) (28). Similar to glutamine deprivation the GAs JHU395 and DON (Figure 1C) inhibited growth of MPNST cells (sNF96.2: JHU395 IC_{50}=4.6 μM; DON IC_{50}=9.8 μM. sNF02.2: JHU395 IC_{50}=1.5 μM; DON IC_{50}=2.4 μM), while growth of immortalized Schwann cells (ipn02.32λ) was minimally affected (Figure 1D; Supplemental Figure 1A). Compared to a positive control (doxorubicin), GA induced less PARP cleavage as a marker of apoptosis in human MPNST cells (Supplemental Figure 1B). Neither GA treatment nor glutamine deprivation significantly diminished basal mitochondrial oxygen consumption rate nor oligomycin-sensitive (ATP-linked) oxygen consumption rate compared to control (Supplemental Figure 1C, D) (30).

JHU395 is a plasma stable lipophilic GA prodrug which delivers DON to MPNST in vitro and in vivo.

Multiple investigations were carried out to characterize JHU395 as a prodrug GA to be used for MPNST. JHU395 showed improved passive permeability compared to DON (DON $P_{app}=0.0095 \times 10^{-6}$ cm/sec vs JHU395 $P_{app}=5.707 \times 10^{-6}$ cm/sec) (Figure 2A). Over 80% of JHU395 remained intact following a one hour incubation in plasma of multiple species,

including humans (Figure 2B). In an *in vitro* plasma to tumor cell partitioning assay measuring JHU395 delivery of DON to human MPNST cells, 92% of total DON measured after one hour incubation was in cells, with only 8% in plasma (Figure 2C). Consistent with prior experiments, intact JHU395 was detected in the plasma after one hour, and minimal intact JHU395 was measured in MPNST cells (Figure 2C). As reported for other GA prodrugs (25), similar profiles for JHU395 delivery of DON to tumor cells were observed in a lymphoma cell line (Supplemental Figure 2A).

To study JHU395 in MPNST *in vivo*, a flank tumor model was utilized with cells harvested from tumor originating in the NPcis mouse (29). Cells injected subcutaneously to B6 mice developed into tumors that had characteristics of high-grade human peripheral nerve sheath tumors (38) including high cellularity and marked nuclear pleomorphism (Figure 3A). Tumors also exhibited many Ki67 positive cells, and tumor cells were positive for phospho-ERK (Figure 3A).

During our prior experiences with DON in murine models of human disease (24, 39), doses over 0.6 mg/kg daily resulted in weight loss approaching 20% by treatment days 6–7. Based on these experiments, we piloted an oral dosing paradigm of JHU395 1.2 mg/kg (0.45 mg/kg DON equivalent) for five days, followed by 0.5 mg/kg p.o. daily thereafter. In a cohort of non-tumored NPcis mice this regimen was well-tolerated for over thirty days (Supplemental Figure 4A). When flank tumored mice received oral JHU395 at 1.2 mg/kg, the drug was rapidly absorbed and converted to DON with a tumor C_{max} of 1.8 nmol/g and a 2.5:1 tumor-to-plasma AUC ratio (tumor AUC 2.496 hr•nmol/g; plasma AUC 0.977 hr•nmol/ml; Figure 2D). By contrast the small intestine-to-plasma DON ratio was 0.20 thirty minutes after JHU395 oral dosing (jejunum 0.18 nmol/g; plasma 0.91 nmol/ml; $p \leq 0.0001$; Figure 2E). Full time-dependent pharmacokinetic analysis of JHU395 in mice also showed no accumulation of DON in GI tissue versus plasma (Supplemental Figure 2B).

Oral JHU395 decreases murine MPNST growth, blocks glutamine utilization, and causes no overt GI- or neuro-toxicities.

Mice with flank MPNST (n = 10/group; average tumor size of 300 mm^3) were treated with vehicle or JHU395 for 14 days (1.2 mg/kg p.o. × 5 days, 0.5 mg/kg × 9 days). JHU395 significantly inhibited growth of tumors compared to vehicle (1045 mm^3 vs 1695 mm^3; $p \leq 0.05$ Figure 3B). At the conclusion of the experiment a subset of tumors were analyzed by histology and immunohistochemistry. No apparent differences were observed in terms of necrosis or overall cellularity on hematoxylin and eosin staining. No significant changes were observed between the groups in markers of proliferation (e.g. Ki67 staining) or apoptotic cell death (e.g. cleaved caspase 3 staining) (Supplemental Figure 3A, 3B). We then moved to examine metabolite biomarkers of glutamine utilization in tumors. JHU395 induced significant increases in tumor glutamine (vehicle 1293 nmol/g vs JHU395 2096 nmol/g; $p \leq 0.001$) and plasma glutamine (vehicle 475 nmol/ml vs JHU395 729 nmol/ml; $p \leq 0.0001$), confirming inhibition of glutamine utilization (Figure 3C). To assess whether the plasma glutamine changes were arising from the tumor, JHU395 was also administered to non-tumored mice (Supplemental Figure 3C). JHU395 caused a 25% increase in plasma

glutamine in non-tumored mice (vehicle 830 nmol/ml vs JHU395 1036 nmol/ml; p≤0.01), suggesting some inhibition of glutamine metabolism in non-tumor tissues.

Given the past GI-toxicity associated with DON (40–42) and the enhanced lipophilicity of JHU395 (23), mice were assessed for both GI and neurotoxicity over 14 days of oral dosing. JHU395-treated mice remained within 10% of starting weight throughout the experiment (Figure 4A). Vehicle-treated mice gained weight, likely related to tumor growth (average tumor volume = 1695 mm^3 at 14 days). No differences were observed between JHU395- and vehicle-treated jejunal histology, performed on a subset of animals (Figure 4B), nor were significant differences observed in liver transaminases or bilirubin (Figure 4C). With respect to neurotoxicity, no gross changes nor cortical vacuolization were observed on a subset of brains postmortem (Figure 5A). JHU395- and vehicle-treated mice performed similarly on the modified Irwin battery of behavioral assays examining autonomic and somatomotor function (Figure 5B) (43), whereas the positive control oxotremorine induced significant adverse effects. Grip time from an inverted wire was also unaffected by JHU395 (Figure 5C).

JHU395 affects multiple glutamine-dependent metabolites with prominent effects on purine synthesis

To evaluate the effect of JHU395 on glutamine-dependent biosynthesis in MPNST, tumor metabolomics was performed. Among ~400 polar metabolites analyzed, 18 showed statistically significant fold-change with threshold > 2 when compared between vehicle- and JHU395-treated tumors (Figure 6A, Supplemental Table 1). Effects were observed on metabolites in multiple pathways including nucleotide (purine and pyrimidine) synthesis, amino acid metabolism, and hexosamine biosynthesis. The most significantly affected metabolite was N-formylglycinamide ribonucleotide (FGAR), a precursor in *de novo* purine biosynthesis. Prior studies have identified the FGAR amidotransferase as a target of DON (44). In an independent quantitative bioanalytical assay FGAR was 75-fold higher in JHU395-treated tumors compared to vehicle (vehicle 3.4 nmol/g vs JHU395 254.4 nmol/g; p≤0.01; Figure 6B). Since FGAR is a proximal metabolite in purine synthesis, we investigated the acute downstream effects of FGAR blockade in MPNST by *in vivo* stable isotope labeled flux analysis (Figure 6C). Using $^{15}N_2$-glutamine, we traced glutamine incorporation to *de novo* purine synthesis. In tumors harvested from JHU395-treated mice, multiple products of purine synthesis (e.g. inosine, adenosine, and guanosine monophosphates) had significantly lower enrichment of isotopologues from m+1, m+2 (IMP, AMP), or m+3 (GMP) pools compared to vehicle-treated tumors (Figure 6C). Growth of human MPNST cells was partially rescued from JHU395 by cotreatment with GMP (Control JHU395 IC_{50}=6.7 μM; GMP JHU395 IC_{50}=17.0 μM; Figure 6D). Consistent with the global metabolomics data, which did not suggest significant changes to levels of TCA cycle metabolites following JHU395 treatment, tracing $^{13}C_5$-glutamine within JHU395-treated tumors did not show significant differences in enrichment of newly synthesized m+5 (glutamate, alpha-ketoglutarate), or m+4 (succinate) isotopologues compared to vehicle-treated tumors (Supplemental Figure 5A).

Discussion

The studies presented here have characterized glutamine utilization in MPNST and found that, consistent with a prior study (27), human MPNST cells are glutamine dependent. The novel GA prodrug JHU395 demonstrated plasma stability, delivered DON to MPNST cells, and inhibited growth of human MPNST cells in culture. *In vivo* oral JHU395 delivered DON to tumor tissues. Chronic oral administration of JHU395 significantly decreased growth of murine MPNST with limited signs of weight loss and no overt intestinal-, hepato-, or neurotoxicity, largely avoiding the GI toxicity previously reported for DON (17, 24, 39). Future studies will investigate alternative regimens of JHU395 for tolerability and efficacy to maximize treatment duration at the higher (1.2 mg/kg) dose, when tumor growth inhibition was most pronounced.

In vivo JHU395 treatment induced significant increases in tumor and plasma glutamine, presumably by decreasing overall glutamine utilization. Broad assessment of metabolomic changes in JHU395-treated MPNST revealed a substantial increase in the purine precursor FGAR. The enzyme that converts FGAR to the next purine synthetic intermediate, formylglycinamidine ribonucleotide (FGAM), is a glutamine amidotransferase previously shown to be inhibited by DON at low micromolar levels (44). Stable isotope labeled flux analysis using a $^{15}N_2$-glutamine tracer confirmed that JHU395 decreased incorporation of glutamine-derived nitrogen to multiple purine products (IMP, AMP, GMP). Supplementation with GMP partially rescued JHU395-mediated growth inhibition of human MPNST cells, confirming a role for glutamine-requiring purines. In future studies it will be of interest to investigate the relationships between glutamine utilization, purine synthesis, and the genetic changes (e.g. *NF1* loss, inactivation of *CDKN2A* or *TP53*, mutation in *SUZ12*) associated with MPNST development (45).

The active GA in JHU395 is an irreversible inhibitor of multiple glutamine utilizing enzymes (19, 46), and global metabolomics showed that multiple metabolites including nucleotides, hexosamines, and amino acid metabolites were affected by JHU395 treatment of MPNST. Several of these metabolites were also affected upon DON treatment of leukemia cells (46); future work will be needed to investigate their significance in MPNST biology. Interestingly, while the glutaminase II pathway product alpha-ketoglutaramate (47) was increased upon JHU395 treatment of MPNST (Figure 6A, Supplemental Table 1), JHU395 did not acutely affect incorporation of $^{13}C_5$-glutamine derived carbons to TCA cycle intermediates (glutamate, alpha-ketoglutarate, succinate), consistent with its limited effect on oxygen consumption in human MPNST cells. Of note, single agent glutaminase inhibition with twice-daily dosed CB-839 partially decreased MPNST xenograft growth (27) suggesting that MPNST may be susceptible to inhibition at multiple points in glutamine metabolism.

Broadly active GAs inhibit purine metabolism in humans with gout (48), but the data presented here are to our knowledge the first *in vivo* studies to suggest that inhibiting glutamine-dependent purine synthesis may be a potential therapeutic approach for MPNST. An early clinical study combined DON with 6-mercaptopurine (6-MP) in pediatric leukemia with promising results (49). While 6-MP given as a prolonged infusion led to disease

stabilization in approximately 25% of refractory pediatric sarcomas (50), the novel combination of 6-MP and prodrug GA has not been reported as a clinical antisarcoma strategy. As JHU395 is well-tolerated in preclinical studies, it is primed to combine with additional agents to target metabolic susceptibilities of MPNST.

Supplementary Material

Refer to Web version on PubMed Central for supplementary material.

Acknowledgements

We are grateful to Dr. Verena Staedtke for NPcis mice as well as the NPcis tumor-derived cells. We thank Marc Ferrer (NCATS) for ipn02.32λ cells, and Dr. Ahmet Hoke and Weiran Chen for use of the Seahorse metabolic analyzer. The FGAR standard was generously provided by Dr. Qi Sun (Jiangxi Science and Technology Normal University, China). We thank Marigo Stathis, Nadine Forbes McBean, Kristen Lecksell, Sebastien Monette (MSKCC), and Kasia Broniowska (Metabolon) for technical support. We thank Dr. Brad Poore for helpful discussions regarding metabolomics analyses and James Vornov for critical reading.

Financial Support: This work was supported by NIH T32CA060441, and awards from the Pablove Foundation Childhood Cancer Research Seed Grant, and the Rally Foundation/Open Hands Overflowing Hearts Fellowship (to KML); grant LTAUSA18166 by the Ministry of Education, Youth and Sports of the Czech Republic, program INTER-EXCELLENCE (to PM) and by the Institute of Organic Chemistry and Biochemistry of the Academy of Sciences of the Czech Republic, vvi (RVO 61388963); and NIH R01NS103927, the Bloomberg-Kimmel Institute for Cancer Immunotherapy, and a Children's Cancer Foundation Grant (to BSS). Ki67 and cleaved caspase 3 staining were performed in collaboration with the Laboratory of Comparative Pathology of Memorial Sloan Kettering Cancer Center, which was supported in part by National Cancer Institute Cancer Center Support Grant P30CA008748.

References

1. Altman BJ, Stine ZE, Dang CV. From Krebs to clinic: glutamine metabolism to cancer therapy. Nat Rev Cancer. 2016;16:619–34. [PubMed: 27492215]
2. DeBerardinis RJ, Mancuso A, Daikhin E, Nissim I, Yudkoff M, Wehrli S, et al. Beyond aerobic glycolysis: transformed cells can engage in glutamine metabolism that exceeds the requirement for protein and nucleotide synthesis. Proc Natl Acad Sci U S A. 2007;104:19345–50. [PubMed: 18032601]
3. Cluntun AA, Lukey MJ, Cerione RA, Locasale JW. Glutamine Metabolism in Cancer: Understanding the Heterogeneity. Trends Cancer. 2017;3:169–80. [PubMed: 28393116]
4. Yuneva M, Zamboni N, Oefner P, Sachidanandam R, Lazebnik Y. Deficiency in glutamine but not glucose induces MYC-dependent apoptosis in human cells. J Cell Biol. 2007;178:93–105. [PubMed: 17606868]
5. Son J, Lyssiotis CA, Ying H, Wang X, Hua S, Ligorio M, et al. Glutamine supports pancreatic cancer growth through a KRAS-regulated metabolic pathway. Nature. 2013;496:101–5. [PubMed: 23535601]
6. Tajan M, Hock AK, Blagih J, Robertson NA, Labuschagne CF, Kruiswijk F, et al. A Role for p53 in the Adaptation to Glutamine Starvation through the Expression of SLC1A3. Cell Metab. 2018;28:721–36 e6. [PubMed: 30122553]
7. Mathur D, Stratikopoulos E, Ozturk S, Steinbach N, Pegno S, Schoenfeld S, et al. PTEN Regulates Glutamine Flux to Pyrimidine Synthesis and Sensitivity to Dihydroorotate Dehydrogenase Inhibition. Cancer Discov. 2017;7:380–90. [PubMed: 28255082]
8. Davidson SM, Papagiannakopoulos T, Olenchock BA, Heyman JE, Keibler MA, Luengo A, et al. Environment Impacts the Metabolic Dependencies of Ras-Driven Non-Small Cell Lung Cancer. Cell Metab. 2016;23:517–28. [PubMed: 26853747]
9. Yang L, Achreja A, Yeung TL, Mangala LS, Jiang D, Han C, et al. Targeting Stromal Glutamine Synthetase in Tumors Disrupts Tumor Microenvironment-Regulated Cancer Cell Growth. Cell Metab. 2016;24:685–700. [PubMed: 27829138]

10. Evans DG, Baser ME, McGaughran J, Sharif S, Howard E, Moran A. Malignant peripheral nerve sheath tumours in neurofibromatosis 1. Journal of medical genetics. 2002;39:311–4. [PubMed: 12011145]
11. Uusitalo E, Rantanen M, Kallionpaa RA, Poyhonen M, Leppavirta J, Yla-Outinen H, et al. Distinctive Cancer Associations in Patients With Neurofibromatosis Type 1. J Clin Oncol. 2016;34:1978–86. [PubMed: 26926675]
12. Stewart DR, Korf BR, Nathanson KL, Stevenson DA, Yohay K. Care of adults with neurofibromatosis type 1: a clinical practice resource of the American College of Medical Genetics and Genomics (ACMG). Genet Med. 2018;20:671–82. [PubMed: 30006586]
13. Farid M, Demicco EG, Garcia R, Ahn L, Merola PR, Cioffi A, et al. Malignant peripheral nerve sheath tumors. Oncologist. 2014;19:193–201. [PubMed: 24470531]
14. Staedtke V, Bai RY, Blakeley JO. Cancer of the Peripheral Nerve in Neurofibromatosis Type 1. Neurotherapeutics : the journal of the American Society for Experimental NeuroTherapeutics. 2017;14:298–306. [PubMed: 28349408]
15. Kattan MW, Leung DH, Brennan MF. Postoperative nomogram for 12-year sarcoma-specific death. J Clin Oncol. 2002;20:791–6. [PubMed: 11821462]
16. Huber KR, Mayer EP, Mitchell DF, Roberts J. Cell cycle phase perturbations by 6-diazo-5-oxo-L-norleucine and acivicin in normal and neoplastic human cell lines. Br J Cancer. 1987;55:653–6. [PubMed: 3620309]
17. Olsen RR, Mary-Sinclair MN, Yin Z, Freeman KW. Antagonizing Bcl-2 family members sensitizes neuroblastoma and Ewing's sarcoma to an inhibitor of glutamine metabolism. PLoS One. 2015;10:e0116998. [PubMed: 25615615]
18. Wang SZ, Poore B, Alt J, Price A, Allen SJ, Hanaford AR, et al. Unbiased metabolic profiling predicts sensitivity of high MYC-expressing atypical teratoid/rhabdoid tumors to glutamine inhibition with 6-diazo-5-oxo-L-norleucine. Clin Cancer Res. 2019.
19. Lemberg KM, Vornov JJ, Rais R, Slusher BS. We're Not "DON" Yet: Optimal Dosing and Prodrug Delivery of 6-Diazo-5-oxo-L-norleucine. Mol Cancer Ther. 2018;17:1824–32. [PubMed: 30181331]
20. Catane R, Von Hoff DD, Glaubiger DL, Muggia FM. Azaserine, DON, and azotomycin: three diazo analogs of L-glutamine with clinical antitumor activity. Cancer Treat Rep. 1979;63:1033–8. [PubMed: 380801]
21. Tabernero J, Rojo F, Calvo E, Burris H, Judson I, Hazell K, et al. Dose- and schedule-dependent inhibition of the mammalian target of rapamycin pathway with everolimus: a phase I tumor pharmacodynamic study in patients with advanced solid tumors. J Clin Oncol. 2008;26:1603–10. [PubMed: 18332469]
22. Hensley CT, Wasti AT, DeBerardinis RJ. Glutamine and cancer: cell biology, physiology, and clinical opportunities. J Clin Invest. 2013;123:3678–84. [PubMed: 23999442]
23. Nedelcovych MT, Tenora L, Kim BH, Kelschenbach J, Chao W, Hadas E, et al. N-(Pivaloyloxy)alkoxy-carbonyl Prodrugs of the Glutamine Antagonist 6-Diazo-5-oxo-l-norleucine (DON) as a Potential Treatment for HIV Associated Neurocognitive Disorders. J Med Chem. 2017;60:7186–98. [PubMed: 28759224]
24. Rais R, Jancarik A, Tenora L, Nedelcovych M, Alt J, Englert J, et al. Discovery of 6-Diazo-5-oxo-l-norleucine (DON) Prodrugs with Enhanced CSF Delivery in Monkeys: A Potential Treatment for Glioblastoma. J Med Chem. 2016;59:8621–33. [PubMed: 27560860]
25. Tenora L, Alt J, Dash RP, Gadiano AJ, Novotna K, Veeravalli V, et al. Tumor-Targeted Delivery of 6-Diazo-5-oxo-l-norleucine (DON) Using Substituted Acetylated Lysine Prodrugs. J Med Chem. 2019;62:3524–38. [PubMed: 30892035]
26. Malone CF, Fromm JA, Maertens O, DeRaedt T, Ingraham R, Cichowski K. Defining key signaling nodes and therapeutic biomarkers in NF1-mutant cancers. Cancer Discov. 2014;4:1062–73. [PubMed: 24913553]
27. Sheikh TN, Patwardhan PP, Cremers S, Schwartz GK. Targeted inhibition of glutaminase as a potential new approach for the treatment of NF1 associated soft tissue malignancies. Oncotarget. 2017;8:94054–68. [PubMed: 29212209]

28. Li H, Chang LJ, Neubauer DR, Muir DF, Wallace MR. Immortalization of human normal and NF1 neurofibroma Schwann cells. Lab Invest. 2016;96:1105–15. [PubMed: 27617404]
29. Cichowski K, Shih TS, Schmitt E, Santiago S, Reilly K, McLaughlin ME, et al. Mouse models of tumor development in neurofibromatosis type 1. Science. 1999;286:2172–6. [PubMed: 10591652]
30. Divakaruni AS, Paradyse A, Ferrick DA, Murphy AN, Jastroch M. Analysis and interpretation of microplate-based oxygen consumption and pH data. Methods Enzymol. 2014;547:309–54. [PubMed: 25416364]
31. National Research Council (U.S.). Committee for the Update of the Guide for the Care and Use of Laboratory Animals., Institute for Laboratory Animal Research (U.S.), National Academies Press (U.S.) Guide for the care and use of laboratory animals. 8th ed. Washington, D.C.: National Academies Press,; 2011 p. xxv, 220 p.
32. Wohnsland F, Faller B. High-throughput permeability pH profile and high-throughput alkane/water log P with artificial membranes. J Med Chem. 2001;44:923–30. [PubMed: 11300874]
33. Mathiasen JR, Moser VC. The Irwin Test and Functional Observational Battery (FOB) for Assessing the Effects of Compounds on Behavior, Physiology, and Safety Pharmacology in Rodents. Curr Protoc Pharmacol. 2018;83:e43. [PubMed: 30179315]
34. Evans A, Bridgewater B, Liu Q, Mitchell M, Robinson R, Dai H, et al. High Resolution Mass Spectrometry Improves Data Quantity and Quality as Compared to Unit Mass Resolution Mass Spectrometry in High-Throughput Profiling Metabolomics. Metabolomics. 2014;4.
35. Dehaven CD, Evans AM, Dai H, Lawton KA. Organization of GC/MS and LC/MS metabolomics data into chemical libraries. J Cheminform. 2010;2:9. [PubMed: 20955607]
36. Xia J, Wishart DS. Using MetaboAnalyst 3.0 for Comprehensive Metabolomics Data Analysis. Curr Protoc Bioinformatics. 2016;55:14 0 1–0 91.
37. Zheng XA, Wang R, Gong SS, Kong R, Liu R, Sun Q. An efficient and practical synthesis of formylglycinamide ribonucleotide (FGAR). Nucleosides Nucleotides Nucleic Acids. 2018;37:79–88. [PubMed: 29376768]
38. Stemmer-Rachamimov AO, Louis DN, Nielsen GP, Antonescu CR, Borowsky AD, Bronson RT, et al. Comparative pathology of nerve sheath tumors in mouse models and humans. Cancer Res. 2004;64:3718–24. [PubMed: 15150133]
39. Potter MC, Baxter VK, Mathey RW, Alt J, Rojas C, Griffin DE, et al. Neurological sequelae induced by alphavirus infection of the CNS are attenuated by treatment with the glutamine antagonist 6-diazo-5-oxo-l-norleucine. J Neurovirol. 2015;21:159–73. [PubMed: 25645378]
40. Magill GB, Myers WP, Reilly HC, Putnam RC, Magill JW, Sykes MP, et al. Pharmacological and initial therapeutic observations on 6-diazo-5-oxo-1-norleucine (DON) in human neoplastic disease. Cancer. 1957;10:1138–50. [PubMed: 13489662]
41. Lynch G, Kemeny N, Casper E. Phase II evaluation of DON (6-diazo-5-oxo-L-norleucine) in patients with advanced colorectal carcinoma. Am J Clin Oncol. 1982;5:541–3. [PubMed: 7180833]
42. Earhart RH, Amato DJ, Chang AY, Borden EC, Shiraki M, Dowd ME, et al. Phase II trial of 6-diazo-5-oxo-L-norleucine versus aclacinomycin-A in advanced sarcomas and mesotheliomas. Invest New Drugs. 1990;8:113–9. [PubMed: 2188926]
43. Byun NE, Grannan M, Bubser M, Barry RL, Thompson A, Rosanelli J, et al. Antipsychotic drug-like effects of the selective M4 muscarinic acetylcholine receptor positive allosteric modulator VU0152100. Neuropsychopharmacology. 2014;39:1578–93. [PubMed: 24442096]
44. Levenberg B, Melnick I, Buchanan JM. Biosynthesis of the purines. XV. The effect of aza-L-serine and 6-diazo-5-oxo-L-norleucine on inosinic acid biosynthesis de novo. J Biol Chem. 1957;225:163–76. [PubMed: 13416227]
45. Kim A, Stewart DR, Reilly KM, Viskochil D, Miettinen MM, Widemann BC. Malignant Peripheral Nerve Sheath Tumors State of the Science: Leveraging Clinical and Biological Insights into Effective Therapies. Sarcoma. 2017;2017:7429697. [PubMed: 28592921]
46. Lyons SD, Sant ME, Christopherson RI. Cytotoxic mechanisms of glutamine antagonists in mouse L1210 leukemia. J Biol Chem. 1990;265:11377–81. [PubMed: 2358467]

47. Udupa S, Nguyen S, Hoang G, Nguyen T, Quinones A, Pham K, et al. Upregulation of the Glutaminase II Pathway Contributes to Glutamate Production upon Glutaminase 1 Inhibition in Pancreatic Cancer. Proteomics. 2019:e1800451. [PubMed: 31231915]

48. Grayzel AI, Seegmiller JE, Love E. Suppression of uric acid synthesis in the gouty human by the use of 6-diazo-5-oxo-L-norleucine. J Clin Invest. 1960;39:447–54. [PubMed: 13829149]

49. Sullivan MP, Beatty EC Jr., Hyman CB, Murphy ML, Pierce MI, Severo NC. A comparison of the effectiveness of standard dose 6-mercaptopurine, combination 6-mercaptopurine and DON, and high-loading 6-mercaptopurine therapies in treatment of the acute leukemias of childhood: results of a coperative study. Cancer Chemother Rep. 1962;18:83–95. [PubMed: 13918321]

50. Adamson PC, Zimm S, Ragab AH, Steinberg SM, Balis F, Kamen BA, et al. A phase II trial of continuous-infusion 6-mercaptopurine for childhood solid tumors. Cancer Chemother Pharmacol. 1990;26:343–4. [PubMed: 2208575]

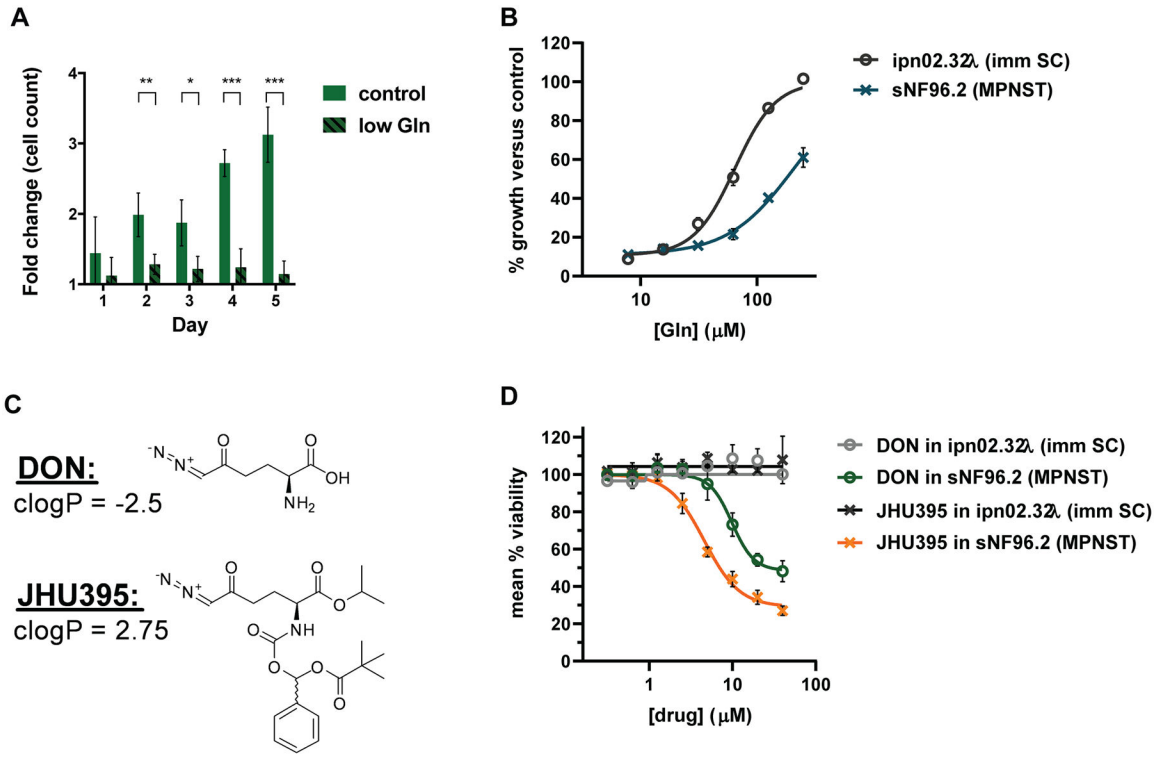

Figure 1:

MPNST cells are sensitive to glutamine deprivation and competitive glutamine antagonists. A) Live cell counts from trypan blue exclusion assay comparing growth of human MPNST cells (sNF96.2) in control (>2mM glutamine) or low (50μM) glutamine media normalized to number of cells seeded. Cells were counted every 24 hours for five days. Data is +/− S.D. B) Percent growth of cells based on alamar blue fluorescence (590 nm) of human MPNST or immortalized Schwann cells (ipn02.32λ; imm SC) growing in glutamine-free media with added glutamine titrated at increasing concentrations. Viability was measured at 72 hours glutamine treatment. Data is +/− S.D. C) Structures of DON and JHU395 with clogP values indicated. D) Percent viable MPNST and immortalized Schwann cells based on alamar blue fluorescence normalized to untreated controls following treatment with DON or JHU395. Viability was measured at 72 hours drug treatment. Data is +/− S.D. *** $0.0001 < p \leq 0.001$, ** $0.001 < p \leq 0.01$, * $0.01 < p \leq 0.05$ by Student's t-test (A).

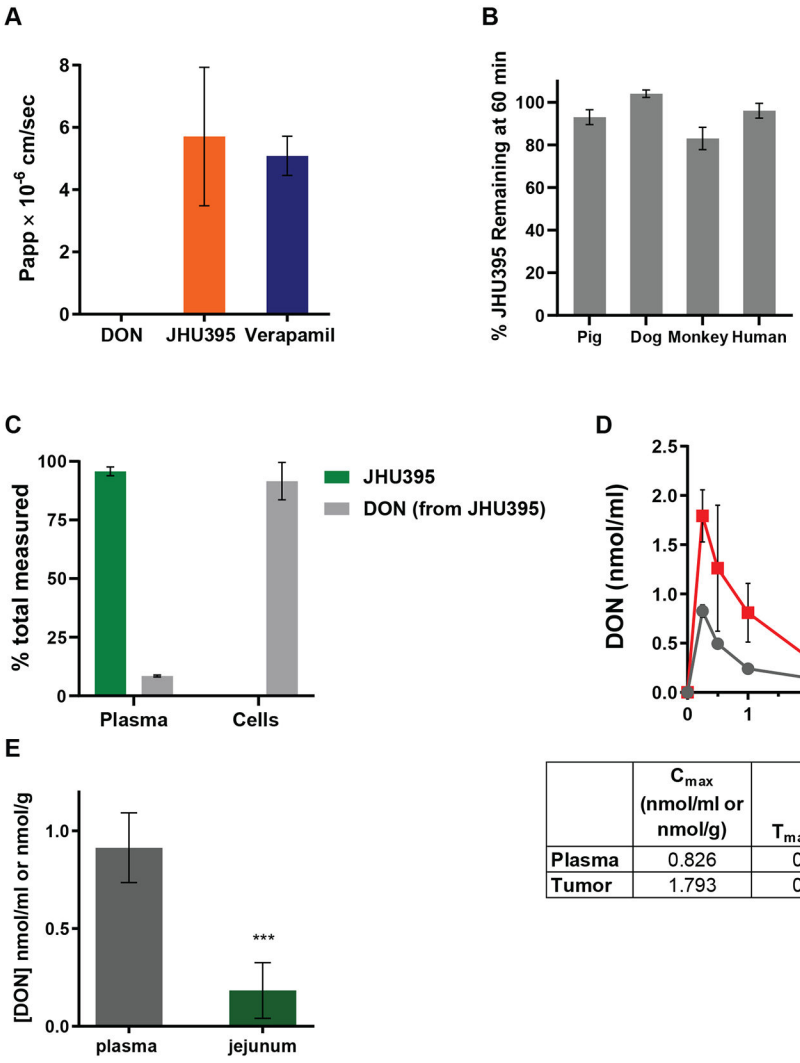

	C_{max} (nmol/ml or nmol/g)	T_{max} (hr)	$AUC_{0->t}$ (hr*nmol/ml or hr*nmol/g)	Ratio (tumor: plasma)
Plasma	0.826	0.25	0.9767	2.57
Tumor	1.793	0.25	2.496	

Figure 2:

JHU395 is a lipophilic, plasma stable prodrug GA that delivers DON to MPNST *in vitro* and *in vivo*. A) Calculated apparent permeability (P_{app}) of DON, JHU395, or Verapamil (positive control) following LC-MS quantification of donor and acceptor samples in a 5 hour parallel artificial membrane permeation assay. Data is +/− S.D. B) Percentage of quantified intact JHU395 in plasma from multiple species following 60 minutes incubation at 37°C. Data is +/− S.D. C) Percentage of quantified intact JHU395 and DON in human plasma and MPNST cells (sNF96.2) following one hour incubation with 20 μM JHU395. Data is +/− S.E.M. D) DON quantification (nmol/g tissue or nmol/ml plasma) following oral administration of 1.2 mg/kg JHU395 to flank MPNST B6 mice. Chart indicates DON C_{max}, T_{max}, and area under the curve (AUC) in tumor and plasma. Error bars are +/− S.D. E) DON quantification (nmol/g tissue or nmol/ml plasma) in plasma and jejunum thirty minutes after 1.2 mg/kg JHU395 to B6 mice. Error bars are +/− S.D. *** $0.0001 < p \leq 0.001$ by Student's t-test.

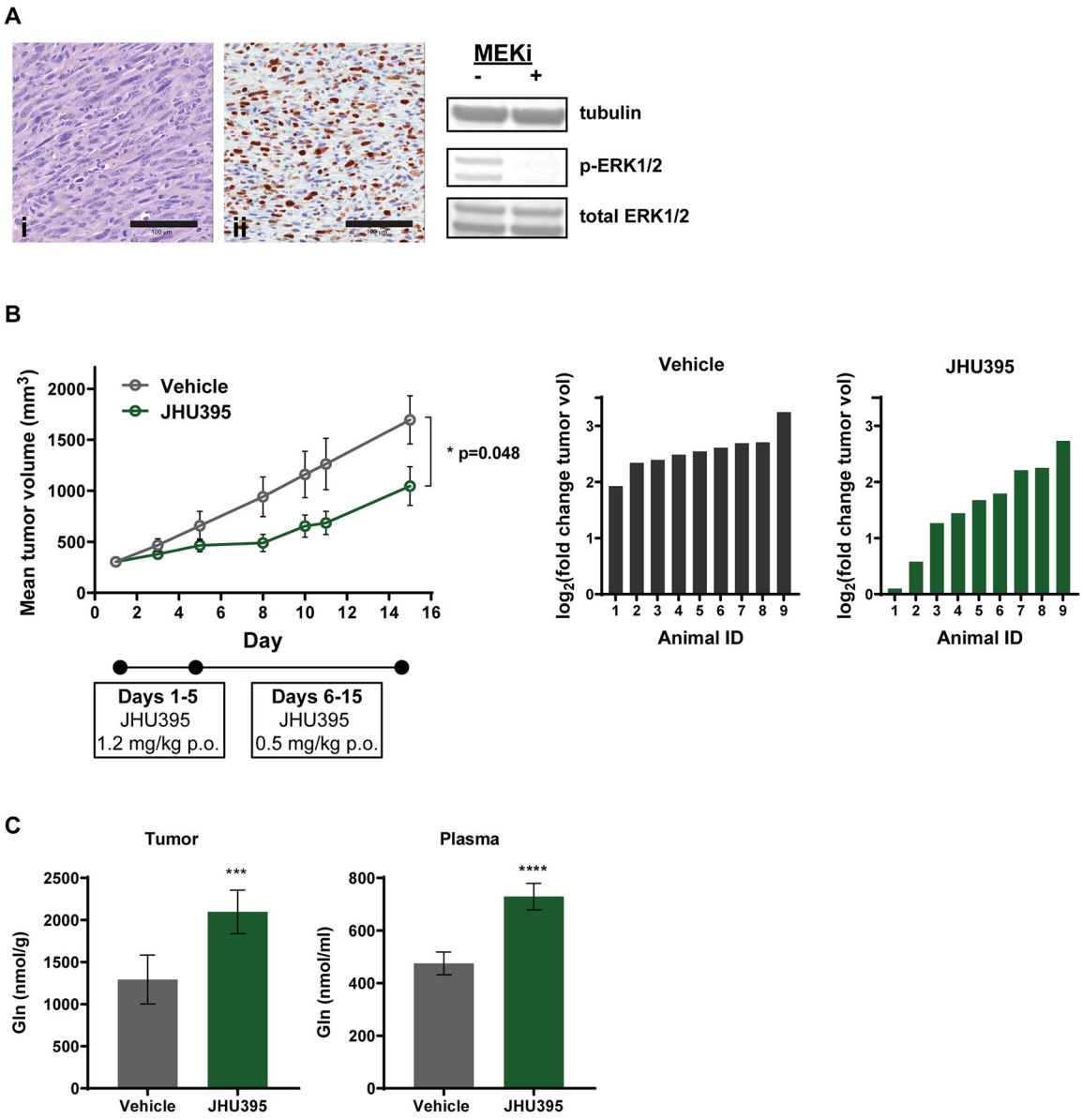

Figure 3:

Orally administered JHU395 decreases tumor growth in a flank MPNST model with concomitant increase in glutamine. A) Characterization of syngeneic murine flank MPNST by H&E stain (i), Ki67 immunohistochemistry (ii), and western blotting for phospho-ERK1/2 in the presence of MEK inhibitor (PD0325901 5μM for 3h). Scalebar on images = 100 μm. B) Mean tumor volumes in mice treated daily with vehicle (grey) or JHU395 (green; 1.2 mg/kg p.o. × 5 days, 0.5 mg/kg p.o. × 9 days). Data shown is mean +/− SEM; * $p \leq 0.05$ by Student's t-test on day 15 and is representative of three independent experiments. Right panels show $\log_2$ (fold change) of individual animal tumor volumes for Day 15 versus Day 1. C) Tumor and plasma glutamine quantified in tissues from JHU395- and vehicle-treated animals. Data shown is mean +/− SD. **** $p \leq 0.0001$, *** $0.0001 < p \leq 0.001$ by Student's t-test.

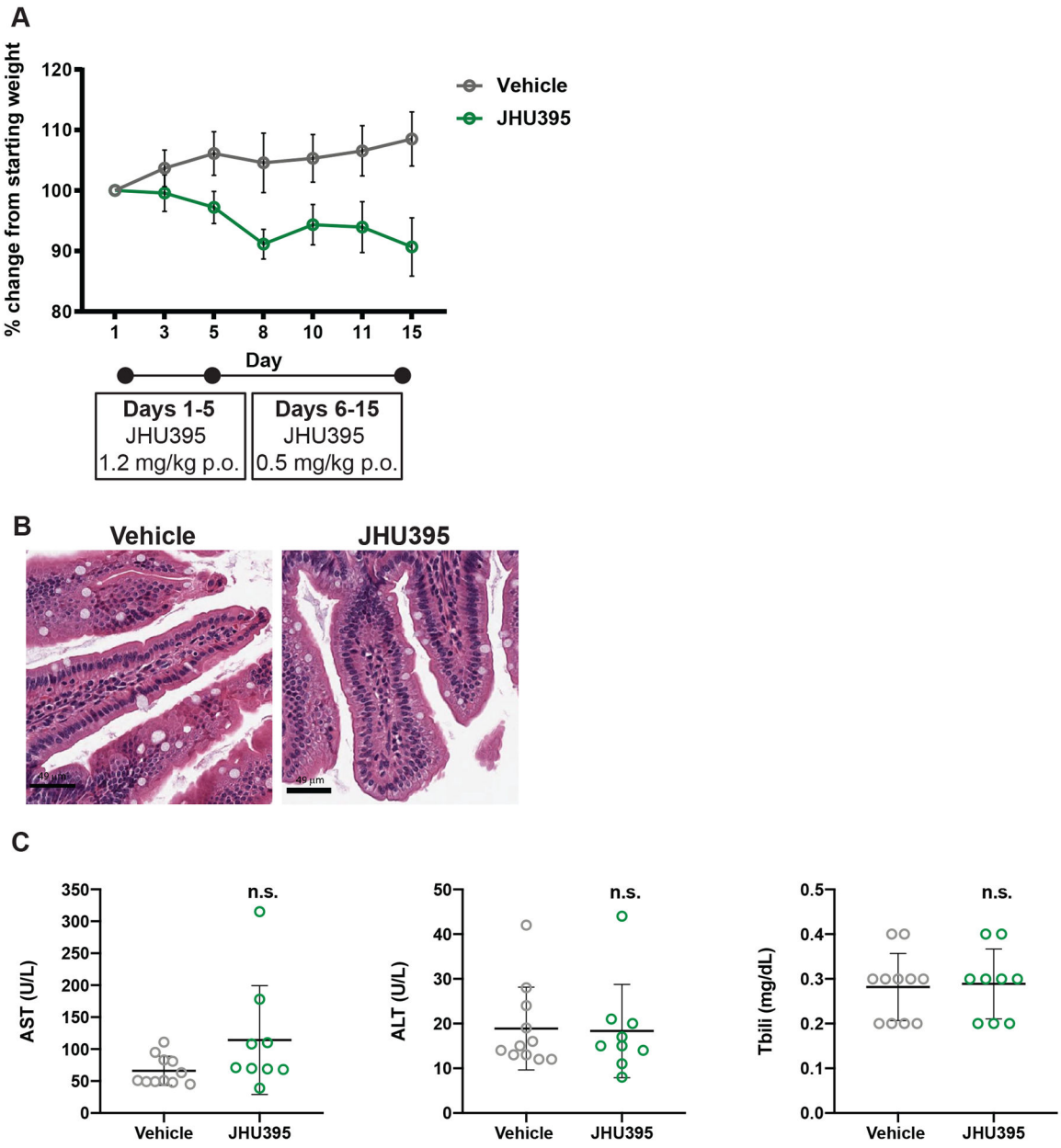

Figure 4:

Orally administered JHU395 has minimal GI or hepatotoxicity. A) Average weight change in flank MPNST mice treated during efficacy study with vehicle or JHU395 (1.2 mg/kg/day p.o. × 5 days, then 0.5 mg/kg p.o. × 9 days; n=9). Change from mean starting weight did not exceed 10%. B) Jejunal histology in a subset of vehicle and JHU395 treated mice after 14 days oral dosing. No increase in apoptotic figures or disruption of crypt architecture was observed. Scalebar = 49 µm. C) Markers of liver toxicity from blood (AST, ALT, total bilirubin) were measured in vehicle or JHU395 treated animals at sacrifice (day 15). All data shown is mean +/− S.D. $p > 0.05$ for each lab value by t-test.

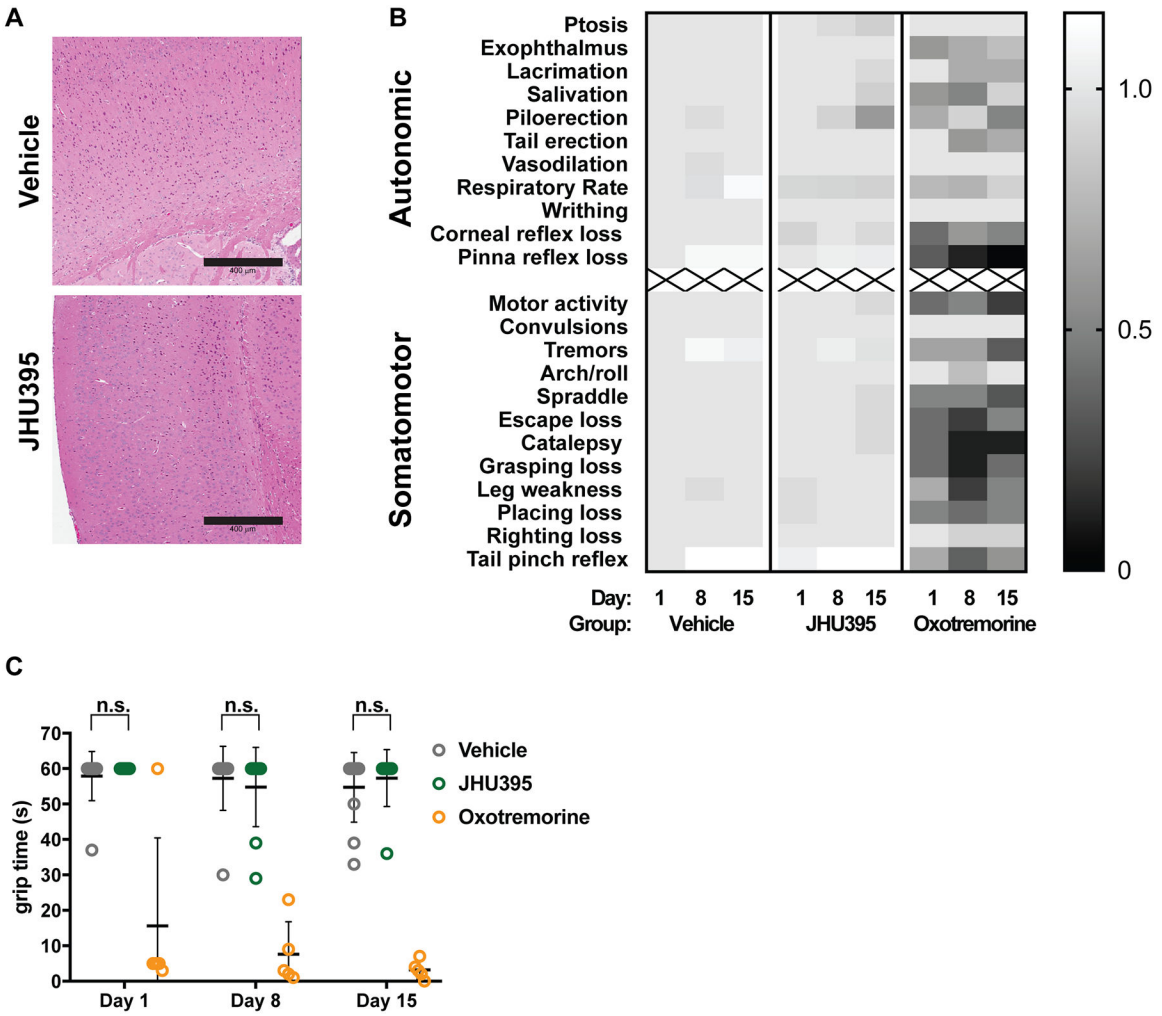

Figure 5:

Orally administered JHU395 has no overt neurotoxicity. A) Brain histology was evaluated in vehicle (PBS + 1% Tween-80 + 2.5% ethanol p.o. daily × 14 days; n=3) and JHU395 (1.2 mg/kg/day p.o. × 5 days, then 0.5 mg/kg p.o. × 9 days; n=3) treated mice. No cortical vacuolization was observed. Scalebar = 400 μm. B) Heatmap showing scoring on modified Irwin behavioral test of vehicle (n=11), JHU395 (n=9), or oxotremorine (n=5; assay positive control) B6 flank MPNST mice over a 14 day dosing period. Mean scores are normalized to day 0 vehicle group and shown per behavior per day. C) Time in seconds that vehicle, JHU395, and oxotremorine treated mice were able to hang from inverted wire in seconds on days 0, 8, and 15 as part of modified Irwin assay. Data shown is mean +/− S.D. $p > 0.05$ for vehicle and JHU395 grip times by multiple t-tests.

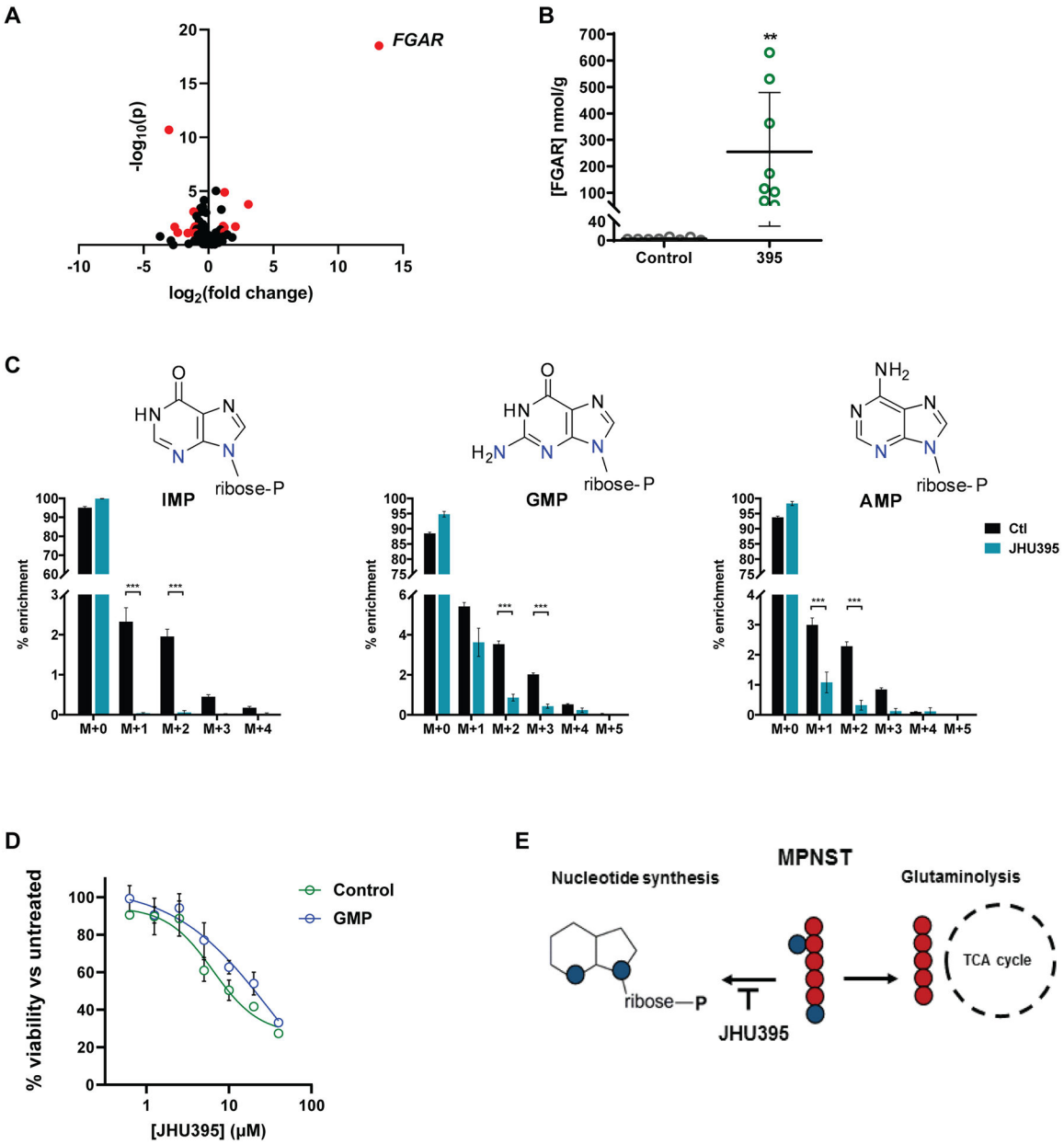

Figure 6:

Metabolomics analyses demonstrate JHU395 inhibition of tumor glutamine utilization in purine synthesis. A) Volcano plot of metabolites identified from murine flank MPNST (n = 8 tumors/group) harvested two hours after oral administration of JHU395 (1.2 mg/kg/dose) or vehicle. Metabolites selected by volcano plot with fold change threshold (x) 2 and t-tests threshold (y) 0.1 are shown in red circles. Both fold changes and p values are log transformed. B) Quantitative LC-MS analysis of FGAR from tumors (n = 8 per group) of vehicle or JHU395 treated murine flank MPNST. Data shown is mean +/− S.D.; $p < 0.01$ by t-test. C) $^{15}N_2$-glutamine labeled JHU395-treated tumors show significantly decreased m+1, m+2 isotopologue enrichment (inosine monophosphate, adenosine monophosphate) and significantly decreased m+2, m+3 isotopologue enrichment (guanosine monophosphate)

compared to vehicle-treated tumors. Data shown is for 6–7 animals per treatment representative of two independent experiments. Graphed data is mean percent enrichment +/− S.D. Statistical testing was done by multiple t-tests where *** $p \leq 0.001$, ** $0.001 < p \leq 0.01$, * $0.01 < p \leq 0.05$. D) Percent viable human MPNST cells (sNF96.2) based on alamar blue fluorescence normalized to untreated controls following treatment with JHU395 in standard media (control) or media containing 100μM guanosine monophosphate (GMP). Viability was measured at 72 hours JHU395 treatment. E) Schematic of JHU395 inhibition of glutamine utilization for nucleotide synthesis versus glutaminolysis in human MPNST.